Predicted Vulnerability of Carbon in Permafrost Peatlands with Future Climate Change and Permafrost Thaw in Western Canada

Treat, Claire C.[1*], Miriam C. Jones[2], Jay Alder[3], A. Britta K. Sannel[4], Philip Camill[5], Steve Frolking[6]

For Special Issue of presentations at 2019 AGU Chapman Carbon-Climate Feedback Conference, to be submitted to JGR-B

[1] Alfred Wegener Institute Helmholtz Center for Polar and Marine Research, Telegrafenburg A45, 14473 Potsdam, Germany

[2] Florence Bascom Geoscience Center, U.S. Geological Survey, Reston, VA USA

[3] Geosciences and Environmental Change Science Center, U.S. Geological Survey, Corvallis, OR USA

[4] Department of Physical Geography and Bolin Centre for Climate Research, Stockholm University, Stockholm, Sweden

[5] Earth and Oceanographic Science Department and Environmental Studies Program, Bowdoin College, Brunswick, ME USA

[6] Institute for the Study of Earth, Oceans, and Space, University of New Hampshire, Durham, NH USA

*Corresponding author email: Claire.treat@awi.de, phone: +49 (331)288-2136

Key points:

- Simulated carbon balance in peatlands with and without permafrost using process-based model from 8000 BP to 2100 CE
- Modeled decomposition losses from active layer peat (0.2 - 1.0 m) was the predominant carbon source, not deeper peat or newly thawed permafrost
- Modeled new peat accumulation offset a large fraction of C losses but future changes in vegetation productivity are poorly understood

Treat, C. C., Jones, M. C., Alder, J., Sannel, A. B. K., Camill, P., & Frolking, S. (2021). Predicted Vulnerability of Carbon in Permafrost Peatlands with Future Climate Change and Permafrost Thaw in Western Canada. Journal of Geophysical Research: Biogeosciences, 126, e2020JG005872. https://doi.org/10.1029/2020JG005872

Abstract

Climate warming in high-latitude regions is thawing carbon-rich permafrost soils, which can release carbon to the atmosphere and enhance climate warming. Using a coupled model of long-term peatland dynamics (Holocene Peat Model, HPM-Arctic), we quantify the potential loss of carbon with future climate warming for six sites with differing climates and permafrost histories in Northwestern Canada. We compared the net carbon balance at 2100 CE resulting from new productivity and the decomposition of active layer and newly-thawed permafrost peats under RCP8.5 as a high-end constraint. Modeled net carbon losses ranged from -3.0 kg C m^{-2} (net loss) to +0.1 kg C m^{-2} (net gain) between 2015 to 2100. Losses of newly thawed permafrost peat comprised 0.2 to 25% (median: 1.6%) of "old" C loss, which were related to the residence time of peat in the active layer before being incorporated into the permafrost, peat temperature, and presence of permafrost. The largest C loss was from the permafrost-free site, not from permafrost sites. C losses were greatest from depths of 0.2 – 1.0 m. New C added to the profile through net primary productivity between 2015-2100 offset ~40% to >100% of old C losses across the sites. Differences between modeled active layer deepening and flooding following permafrost thaw resulted in very small differences in net C loss by 2100, illustrating the important role of present-day conditions and permafrost aggradation history in controlling net C loss.

Plain language summary

The thawing of permafrost in tundra, fen, bog, and other peatland wetlands can enhance climate change through releasing carbon from the soil. Using a model for six sites in western Canada, we estimate how much carbon will be lost by 2100 under a high-end emissions scenario. While these peatlands continue to accumulate carbon in the surface soil layers through enhanced vegetation growth, more carbon is lost from slightly deeper in the soil profile. As a result, most sites were projected to lose relatively small

amounts of carbon compared to how much they contain (< 5%). Little of the carbon lost was from newly thawed permafrost, while the largest carbon losses were from the permafrost-free site. In sites where permafrost thawed, the carbon losses were related to peatland and permafrost history.

Introduction

Peatlands in northern high latitudes store significant amounts of soil carbon (C), estimated at 450 to 1000 Pg C globally [*Gorham*, 1991; *Nichols and Peteet*, 2019]. In northern regions, an estimated 1.22 x 10^6 km^2 of peatland contains permafrost, or 35% of northern peatlands [*Hugelius et al.*, 2020], which protects peat C from decomposition and loss to the atmosphere when the peat is frozen [*Tarnocai*, 2006]. With warming temperatures in northern high latitudes associated with climate change, it is important to understand whether peatlands (and permafrost peatlands) will continue be net C sinks or whether some C stored in long-term peat C reservoirs will be released to the atmosphere and cause feedback to the climate system [*Frolking et al.*, 2011; *Schuur et al.*, 2015]. While factors such as water table position and temperature have long been known to control C exchange in peatlands [*Gorham*, 1991], permafrost peatlands may have some unique controls on C feedbacks. Once peat leaves the active layer and becomes permafrost, any further decomposition is halted until it thaws. Some studies have documented relatively large C losses post-thaw [*Jones et al.*, 2017; *O'Donnell et al.*, 2012], while others have reported minimal losses [*Estop-Aragonés et al.*, 2018a; *Heffernan et al.*, 2020]. In permafrost peatlands, decomposition of newly-thawed peat may be limited by the presence of highly degraded material [*Treat et al.*, 2014] that has limited biogeochemical activity potential [*Estop-Aragonés et al.*, 2018a]. In general terms, the longer peat persists before becoming frozen into permafrost, the more degraded the peat will be, and the less susceptible to decomposition upon subsequent permafrost thaw.

Empirical and experimental approaches to estimating losses of peatland C following permafrost thaw have generated important hypotheses about the controls on C loss from peatlands following permafrost thaw utilizing inter-site comparisons. Based on the analysis of peat types and decomposition rates, and net C losses across a range of sites with different histories, the magnitude of net C loss is hypothesized to be related to the relative timing of permafrost aggradation and peat deposition [*Heffernan et al.*, 2020; *Jones et al.*, 2017; *Treat et al.*, 2014]. For example, chronosequences with relatively large C losses accumulated peat which was quickly incorporated into permafrost over millennia (e.g. syngenetic permafrost formation), resulting in minimally decomposed permafrost peat that is then decomposed more readily upon thaw [*Jones et al.*, 2017; *O'Donnell et al.*, 2012; *Treat et al.*, 2014]. On the other hand, permafrost aggraded more recently in peatlands of Western Canada (Alberta, Manitoba) than in some parts of Alaska [*Treat and Jones*, 2018; *Zoltai and Vitt*, 1990], suggesting that C in permafrost peat was deposited substantially before incorporation into permafrost and therefore subjected to greater decomposition. Results from empirical studies of peatlands in Alberta have shown smaller C losses post thaw [*Estop-Aragonés et al.*, 2018a; *Estop-Aragonés et al.*, 2018b; *Heffernan et al.*, 2020] than in Alaska [*Jones et al.*, 2017; *Plaza et al.*, 2019], offering some support for this hypothesis.

While these losses of permafrost C are estimated using empirical modeling, the C losses from permafrost are difficult to quantify directly using observations. Other *in-situ* processes, such as enhanced net primary productivity in wetter, newly thawed peatlands, may mask any changes in peat C exchange [*Camill et al.*, 2001; *Prater et al.*, 2007; *Turetsky et al.*, 2007]. Detecting the relatively small fluxes of CO_2 or CH_4 from thawing permafrost peat or old, deep peat against the relatively large magnitude of modern ecosystem respiration fluxes can be difficult using radiocarbon or $\delta^{13}C$ isotopic signatures [*Estop-Aragonés et al.*, 2018b], and the interpretation can be ambiguous because of the fractionation associated with decomposition processes [*Dorrepaal et al.*, 2009; *Hicks Pries et al.*, 2015]. Furthermore, there is the complication of high interannual and spatial variability in CO_2 and CH_4 exchange that may mask long-term trends and affects conclusions drawn primarily from growing season measurements [*Roessger et al.*, 2019; *Roulet et al.*, 2007; *Treat et al.*, 2018].

Interactions between temperature, carbon cycling in peatlands, and peatland hydrology are difficult to untangle from field observations. Models can provide insights into how different factors affect overall system behavior. Here, we compare the potential peat C losses with future warming and permafrost thaw at six sites along a temperature and permafrost gradient in Canada, ranging from a permafrost-free site in James Bay Lowland at the edge of discontinuous (sporadic) permafrost zone to the sub-Arctic continuous permafrost zone [*Brown et al.*, 2002]. We use a process-based peatland model, which allows us to examine how different factors, including predicted temperature increases, site wetting and drying, productivity increases, and site permafrost history, combine and interact to affect the peat C balance with warming and permafrost thaw. The goals of this study were to:

- Develop a model of long-term peatland processes and permafrost formation that can be applied at multiple northern sites;
- Predict changes in peat C stocks in response to warming climate for a set of northern sites that span a permafrost gradient;
- Determine what factors (e.g. mean annual air temperature, predicted temperature increase, peat accumulation history, other factors) controlled the change in net C stocks.

Figure 1. Map of site locations included in this permafrost transect study across western Canada, ranging from permafrost-free in the south (JBL3), to discontinuous (Joey Lake, Selwyn Lake), and to continuous permafrost in the north (Ennadai Lake, Baillie Bog, Thelon-Kazan Peatland / TKP). Peat cores from each site were collected as part of individual studies (see Table 1) and analyses were included in an earlier synthesis project [*Treat et al.*, 2016]. The "Discontinuous" permafrost zone here also includes isolated and sporadic permafrost zones. Permafrost zone map source: Brown et al. [2002], treeline from *Olson et al.* [2001].

Site Descriptions

We selected six peatland sites that spanned the range of permafrost conditions in western Canada where previous paleoecological studies have been completed (Figure 1, Table 1). The modern climate of the study region is generally cold continental, with mean annual temperatures below or near 0 °C and less than 750 mm of annual precipitation (Table 1). The peatland sites are located on the Canadian shield, where peatlands formed following glacial retreat and the drainage of proglacial lakes [*Gorham et al.*, 2007]. The southernmost site, JBL3, is a permafrost-free bog site in the James Bay Lowlands with 2.45 m of woody, herbaceous, and moss peat [*Holmquist and MacDonald*, 2014]. Joey Lake Peatland (core JL2), was sampled from a 3 m deep permafrost bog located in a large peatland complex in the isolated and sporadic permafrost zone near Thompson, Manitoba [*Camill et al.*, 2009]. Farther north in discontinuous permafrost, a nearly 2 m deep peat plateau bog composed mainly of *Sphagnum* moss and rootlet peat was sampled adjacent to Selwyn Lake [*Sannel and Kuhry*, 2008; 2009]. About 170 km northeast in the continuous permafrost zone in the boreal-tundra ecotone, a 1.8 m core from a polygonal peat plateau at Ennadai Lake also contained mainly *Sphagnum* moss and rootlet peat overlying fen peat [*Sannel and Kuhry*, 2008; 2009]. Further north of treeline in continuous permafrost, Baillie Bog [*sic*] (BB, core) was sampled from the middle of a high-centered polygonal [fen] peatland located in a bedrock depression that contained ~2 m of Cyperaceae (sedge) peat with occasional depositions of mineral material in the core [*Vardy et al.*, 2005; *Vardy et al.*, 2000]. Thelon-Kazan Peatland (TKP, core TK1P2) was sampled from another high-centered polygon with nearly 2 m of peat that was mainly composed of Cyperaceae with *Sphagnum* in the surface 35 cm and had a relatively high amount of mineral material throughout the core [*Vardy et al.*, 2005; *Vardy et al.*, 2000]. Data available from cores at all sites includes bulk density, carbon or organic matter content, radiocarbon dates, and either of plant macrofossil analysis, a description of peat type, or an interpretation of peatland class. These data were compiled in an earlier synthesis and are available in digital format for download [*Treat et al.*, 2016] (doi: 10.1594/PANGAEA.863697). The dataset key (Variable: Auth.Site.CoreID) for the cores included in this study is as follows: JBL3 (HOL-JLB-03), Joey Lake (CAM-JL-2), Selwyn Lake (SAN-SEL-SL1), Ennadai Lake (SAN-ENL-1), Baillie Bog (VAR-BB-01), and TKP (VAR-TKP-01).

Table 1. Site names, locations, climatic information, peat height, basal ages, and core information for the peat cores used in this study.

Site Name	Peatland type	Latitude (°N)	Longitude (°W)	Permafrost zone	Mean annual air temp. (°C)	Mean annual precip. (mm/y)	Peat height (cm)	Basal age (cal BP)	Fen-bog transition height (cm)
JBL3	Bog	52° 51.62’	89° 55.77’	None	0.5*[a]	728*[a]	245	7760	195
Joey Lake (core JLP2)	Permafrost bog	55° 27.95’	98° 9.80’	Isolated & Sporadic	-2.9*[b]	509*[b]	300	8000	176
Selwyn Lake (core SL1)	Peat plateau margin	59° 53’	104° 12’	Discontinuous	-3.3†	430†	197	6580	22
Ennadai Lake (core EL1)	Peat plateau margin	60° 50’	101° 33’	Continuous (~30 km south of tree-line)	-9†	290†	186	5810	49
Baillie Bog (BB, core BB1)	High-center polygon	64° 42.8’	105° 34.75’	Continuous (200 km N of tree-line)	-10.9*[c]	300 *[c]	197	7750	182‡
Thelon-Kazan Peatland (TKP, core TK1P2)	High-center polygon	66° 27.07’	104° 50.08’	Continuous (400 km N of tree-line)	-11.3*[d]	272*[d]	193	6620	183‡

* Climate normals from Environment Canada (1980-2010) for stations: [a] Pickle Lake A, [b] Thompson A, [c] Lupin A, [d] Baker Lake A; https://climate.weather.gc.ca/climate_normals/; accessed 12 December 2019.

† Sannel & Kuhry 2008, 2009

‡ No clear evidence of fen-bog transition. Here the authors describe a transition from herbaceous to woody species in peat.

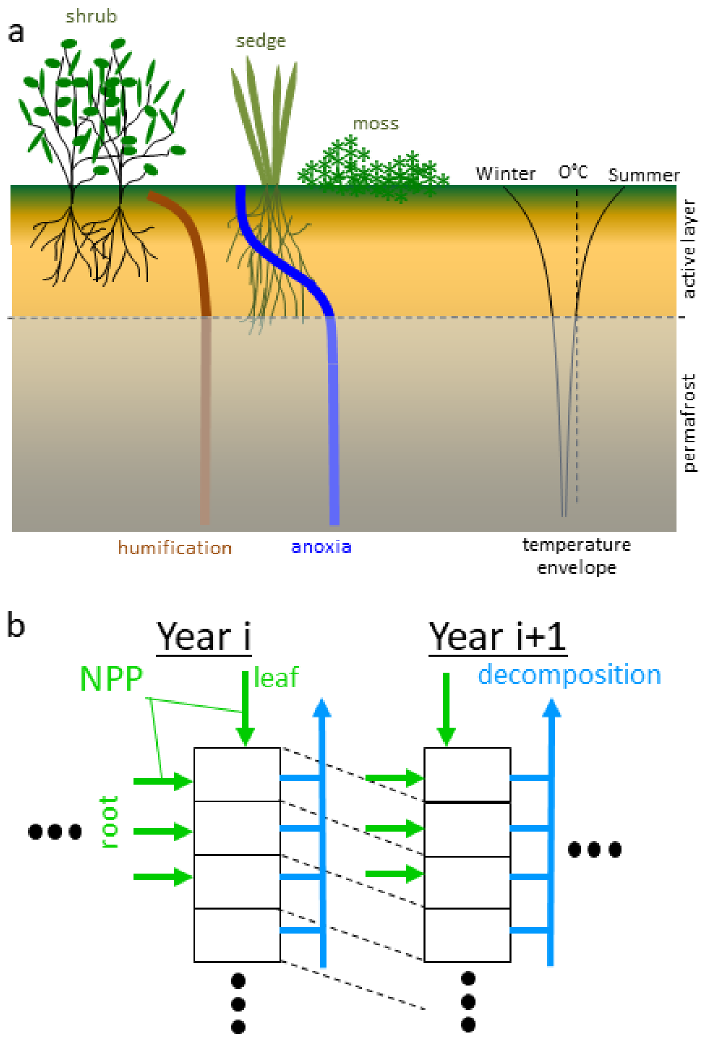

Basic structure of HPM. **(a)** In HPM, relative NPP of three plant functional types – moss, shrub, and sedge – varies with water table depth and active layer thickness. Anoxia profile is determined by depth below water table. Humification profile is determined by fresh root litter inputs and decomposition, as fraction mass remaining. Monthly temperature profiles computed by heat transfer with phase change, including a snowpack layer in winter. Permafrost occurs if T_{soil_layer} <0°C for 24+ consecutive months. **(b)** All annual aboveground net primary productivity (NPP) is added as a surface litter cohort; belowground NPP is added to annual litter/peat cohorts based on rooting depth and profile (limited to active layer). Decomposition rates vary down the peat profile, controlled by litter quality and interacting profiles shown in panel (a). Annual peat cohorts accumulate through millennia of simulation to generate an age-depth profile characterized by relative amounts of moss, sedge, and shrub peat remaining.

Figure 2. Basic structure of HPM. (a) In HPM, relative NPP of three plant functional types – moss, shrub, and sedge – varies with water table depth and active layer thickness. Anoxia profile is determined by depth below water table. Humification profile is determined by fresh root litter inputs and decomposition, as fraction mass remaining. Monthly temperature profiles computed by heat transfer with phase change, including a snowpack layer in winter. Permafrost occurs if Tsoil_layer <0°C for 24+ consecutive months. (b) All annual aboveground net primary productivity (NPP) is added as a surface litter cohort; belowground NPP is added to annual litter/peat cohorts based on rooting depth and profile (limited to active layer). Decomposition rates vary down the peat profile, controlled by litter quality and interacting profiles shown in panel (a). Annual peat cohorts accumulate through millennia of simulation to generate an age-depth profile characterized by relative amounts of moss, sedge, and shrub peat remaining.

Methods

Model description

We used HPM-Arctic to model peat formation since initiation to present and into the future. The HPM-Arctic version integrates two earlier models: The Holocene Peat Model (HPM), a coupled carbon-hydrologic model for peatlands [*Frolking et al.*, 2010], the Geophysical Institute Permafrost Lab soil thermal model GIPL2 [*Marchenko et al.*, 2008]. Briefly, HPM simulates the development of a peat profile over millennia, from initiation, using an annual litter cohort approach so that results can be compared to dated peat cores (Figure 2). Rates of peat accumulation and decomposition are a function of plant community composition (litter quality), modified by dynamic environmental conditions, including water table level and water content in the unsaturated zone, and temperature profiles. Plant community composition (i.e., relative litter inputs from different plant functional types) is dynamic, responding to mean growing season water table depth and peat depth as a proxy for nutrient status. Annual net primary productivity (NPP) is set equal to annual litterfall, the carbon input for peat accumulation. NPP temperature sensitivity was modeled as a Q_{10} function, with a Q_{10} value of 1.8, based on an empirical relationship between mean annual air temperatures and above-ground net primary productivity for mosses, vascular plants, and trees that was developed for a transect of peatland sites in boreal Manitoba, Canada [*Camill et al.*, 2001]. Peat bulk density in HPM is computed for each annual litter/peat cohort, and increases non-linearly from a minimum to a maximum value (50 – 130 kg m^{-3}) as the cohort loses mass through decomposition [*Frolking et al.*, 2010]. The water table level is calculated from a simple water balance model (precipitation minus evapotranspiration plus net run-on/run-off, and the net peat water content determines the water table location, where the peat water content in the unsaturated zone is a function of peat bulk density and distance above the water table [*Frolking et al.*, 2010].

HPM-Arctic has been modified from the original version of HPM in several ways. Principally, it has been coupled to the Geophysical Institute Permafrost Lab soil thermal model GIPL2 [*Marchenko et al.*, 2008], modified to include an accumulating peat layer on the soil surface [GIPL-2-peat; *Treat et al.*, 2013; *Wisser et al.*, 2011]. GIPL-2-peat is a soil thermal model that solves vertical soil heat transfer and phase change using a numerical approximation accounting for soil type and soil water content; it is driven by air temperature and includes a dynamic winter snowpack as a heat transfer layer. Soil temperatures are calculated for a 100-m soil and bedrock column that has varying thermal properties with depth and variable layer thicknesses, thinner at the surface (0.05 m minimum) and thicker down the soil column into the bedrock (5 m maximum). As peat accumulates on the soil surface over centuries to millennia (at rates generally < 0.001 m yr^{-1}), the mineral soil and bedrock layers slowly descend deeper into the simulated soil profile. Simulated soil temperatures are used to constrain rates of peat decomposition, and variation in the active layer thickness is used instead of peat depth as an indication of nutrient status, which impacts net primary productivity of vascular plants. Active layer thickness, updated annually, is determined by identifying the soil thermal layer just above the top-most layer where the temperature remains below 0° C for two years continuously, in accordance to the definition of permafrost [*S A Harris et al.*, 1988].

In addition to soil temperature profiles, HPM-Arctic has (i) reduced the model time step from annual to monthly for model drivers (air temperature and precipitation), peat profile water balance, and decomposition (the soil thermal model operates at a daily timestep, using air temperatures interpolated from the monthly values); (ii) reduced the number of plant functional types to three: moss, herbaceous (including sedges and graminoids), and ligneous (woody species including shrubs), where for the vascular plants, the inputs and decomposition of above and belowground litter are tracked separately; and (iii) incorporated a simple ‘old-new’ carbon tracking algorithm, whereby after a specified year all moss, sedge, and shrub plant litter gets labeled as 'new', so that its accumulation as peat and loss through decomposition can be tracked separately from the older peat derived from plant litter inputs prior to the specified year. This study used 2015 CE as both present-day and the boundary between new and old carbon inputs. Model code for these runs and for HPM-Arctic is available for download (doi: 10.5281/zenodo.4647666).

Model optimization and evaluation

Some site-specific calibrations were done for several model parameters to capture variability (often not reported) related to individual watershed and site characteristics (Table 2). Peat initiation often occurs in a local topographic low, receiving run-on from the surrounding watershed; as the peat accumulates and the peat surface rises, it can shift to a local topographic high point, and shed water (run-off) rather than receive it [*Charman*, 2002]. The site-specific model parameters include the accumulating peat height at which this shift from run-on to run-off occurred ($H_{run\text{-}on/off}$), and the peat height when initial fen-type vegetation transitioned to bog-type vegetation (H_{FBT}). When the peat height exceeds the site-specific H_{FBT}, the peatland transitions from a fen to a bog, which involves a decrease in annual NPP to a varying degree [*Rydin and Jeglum*, 2006] modeled with a site specific fractional parameter ($F_{NPP\text{-}bog}$). With greater lateral hydrological flow, and therefore a shorter water residence time in the saturated zone, fen conditions are assigned a longer scale length (e-folding depth below the water table) to a full anoxia impact on decomposition rate [e.g. *Glaser et al.*, 2016]. This is modeled with an anoxia scale length parameter [*Frolking et al.*, 2010], which controls the decline in decomposition rate with depth below the water table, emulating how far/quickly reduced electron acceptors are replenished below the water table. This affects peat decomposition rates below the water table. If/when permafrost is present, frozen peat decomposition rates are set to zero (also for seasonal winter frost), while decomposition persists in the seasonally-thawed surface active layer.

Site-specific parameter values were determined from a combination of observations and/or optimization routines (Table 2). The parameter H_{FBT} was determined by trial and error from the final peat height and observations of the height of the fen-to-bog transitions (H_{FBT}) in the site core profiles; the model parameter H_{FBT} generally was higher than in the observations. $H_{run-on/off}$ was determined by trial and error from the agreement between the modeled peat height and observed peat height, as well as the macrofossil composition, which indicated relative water table position over time (e.g. dry or wet). The other three parameters ($F_{NPP-bog}$, and anoxia scale lengths for fen and bog) were determined from minimizing the root mean squared error between the observed and modeled age-depth profiles, where the age of the peat surface was assumed to be the year of sampling. For most sites, the optimization routine was implemented using the *fmincon* solver in MATLAB. For sites with only two radiocarbon dates (TKP, BB), the parameterization used was based on earlier runs at the next northernmost site (Ennadai) and generalized parameters for temperate and boreal peatlands [*Frolking et al.*, 2010]. To speed up the optimization process, the optimization routine used a simplified model version with a constant time series of peat temperature profiles that was generated using the initial parameter values. After solving for the optimal parameterization, we iterated this procedure by re-running the full model to update the soil temperature profile using the optimized parameters, re-ran the optimization routine, and re-ran the full model for a final time.

For calculating organic matter stocks and C stocks, model output (mass of peat) was multiplied by mean values determined from a synthesis of over 10,000 peat layers spanning the permafrost region [*Treat et al.*, 2016]. The conversion factor from peat to organic matter (OM) was 0.924 g OM g^{-1} peat. The conversion factor from organic matter to carbon was 0.495 g C g^{-1} OM.

We calculated the residence time of peat in the active layer before being incorporated into permafrost. The active layer residence time was dynamic over time, as both peat height and active layer thickness change every year, so this value was determined using the 500-year litter cohorts tracked in HPM. HPM-Arctic tracks several metrics for these 500-year litter cohort markers every year, including the depth below the peat surface and height above the mineral soil surface. We found the height of the permafrost in the peat profile in each year and calculated the year when each litter cohort was first incorporated into the permafrost. Knowing the age of the 500-year litter cohort when it entered the permafrost allowed us to calculate the residence time of that peat cohort in the active layer.

Table 2. Site-specific parameterization used in HPM-Arctic. * Indicates that parameter value was determined using an optimization routine (Optimization methods).

Parameter	Description	JBL3	Joey Lake	Selwyn Lake	Ennadai Lake	Baillie Bog (BB)	Thelon-Kazan (TKP)
$H_{run\text{-}on/off}$	Height run-on/off (m)	1.50	0.31	0.40	0.75	2.2	4.5[a]
H_{FBT}	Height of fen-bog transition (m)	2.0	2.2	0.6	2.2	2.3	2.1
$F_{NPP\text{-}bog}$	NPP multiplier at H_{FBT}	0.73*	0.55	0.55	0.48*	0.48	0.48
AnoxiaScale-$_{Fen}$	anoxia scale length in fen when height < H_{FBT} (m)	1.10*	1.11*	2.46*	2.05*	3.0	3.0
AnoxiaScale$_{\text{-}Bog}$	anoxia scale length in bog when height > H_{FBT} (m)	0.81*	0.28*	1.075*	0.21*	1.2	1.2
Max NPP	Maximum annual NPP under ideal conditions (kg m^{-2} y^{-1}).	1.5	1.5	1.5	1.5	1.1	1.1
Ndates	Number of ^{14}C dates in profile*	6	11	13	4	2	2
RMSE	Root mean square error, model vs. observations	26.4	182.1	70.9	34.1	27.1	21.3

** The age of the peat surface was assumed to be the same as the year of sampling and included in the age-depth model.*
[a] A value deeper than the peat height indicates that the peat will continues to receive run-off until the threshold is reached.

Model scenarios

We explored two possible water table scenarios resulting from warmer soil temperatures and permafrost thaw: perched and flooded. The perched water table scenario reflected a water table perched on top of the permafrost, which results in a drier soil profile as water drains laterally due to differences in elevation. This feature is common in peat plateaus and palsas [*Zoltai*, 1993], which are elevated from the surrounding peatlands from uplift associated with permafrost formation [*Seppälä*, 2011], resulting in water drainage to adjacent lower-lying areas. Because the water table is perched on top of the permafrost, as the depth to permafrost increases with warming soil, the depth to the water table also increases and sites become drier [*Haynes et al.*, 2018; *Osterkamp et al.*, 2009]. No changes were needed to the model setup to reproduce this behavior.

The flooded scenario represents a peatland with thawing permafrost that is receiving water from adjacent uplifted areas [*Osterkamp et al.*, 2009; *Zoltai*, 1993]. This would be fairly analogous to a thermokarst peatland, where the peat surface becomes flooded due to permafrost thaw, ice melt, and resulting subsidence of the peat surface [*Osterkamp et al.*, 2000]. However, while HPM-Arctic simulates frozen peat in the peat profile, it does not simulate the formation or degradation of ice lenses, and it does not account for volume or peat height changes associated with ice formation, accumulation, and thaw [e.g. *Seppälä*, 2011]. Instead, we used the flooding scenario to mimic the lateral redistribution of water from the surrounding peat associated with permafrost thaw and collapse [e.g. *Osterkamp et al.*, 2009; *Seppälä*, 2011] by resetting the $H_{run\text{-}on/off}$ parameter. The new value for $H_{run\text{-}on/off}$ was set to the peat height at the time when two conditions were met: (i) permafrost thaw had reached a mean active layer thickness >1.25 m for the previous 10-year period (active layer thickness greater than 1.25 is not measurable with a typical frost probe and not likely to be detected without intensive GPR surveys), and (ii) peat height decreased (net peat added was less than peat lost over the previous 10-year period). Resetting $H_{run\text{-}on/off}$ to the new peat height had the effect of wetting the peat and bringing the water table near the surface, as is commonly observed in thermokarst features [*Osterkamp et al.*, 2000]. Because the flooding scenario was determined dynamically within the model, not all sites experienced thermokarst flooding, either because the active layer thickness did not exceed 1.25 m or because peat was not lost.

Model climate drivers

We utilize the TraCE-21ka transient simulations [*Liu et al.*, 2009 https://www.earthsystemgrid.org/project/trace.html] to drive HPM-Arctic with monthly temperature and precipitation climate forcings from 8000 B.P. to 1990 CE (8 Kyr time series). The TraCE-21ka simulations are driven by paleo changes in greenhouse gases, insolation, and paleogeography as sea level rises from the melting of the large northern hemisphere ice sheets. Monthly temperature and precipitation time series were extracted from the coarse 3.75° x ~3.75° grid by bilinear interpolation to the six peatland site locations (Figure 1, Table 1). The simple "delta method" bias correction was applied to the TraCE-21ka output by converting the 8 Kyr time series to anomalies relative to 1950-1990 CE and applying the anomalies to a modern observed gridded data set [CRU TS v3.32; *I Harris et al.*, 2014]. TraCE-21ka temperature anomalies are applied additively to modern observations, whereas precipitation anomalies are applied as scalars. To continue the 8 Kyr timeseries into the future, we adopt the CCSM4 RCP8.5 simulation from the Coupled Model Intercomparison Project Phase 5 [CMIP5; *Taylor et al.*, 2012]. The RCP8.5 scenario was chosen as an end-member to bracket the greatest projected changes in temperature and precipitation. CCSM4 [*Gent et al.*, 2011] is the successor to the CCSM3 model used in the TraCE-21ka simulations, which we chose for consistency. While focusing on one model projection is a limitation, CCSM4 has an equilibrium climate sensitivity (the response to a doubling of atmospheric CO_2) of 2.9 °C, which is similar to the CMIP5 ensemble multi-model mean of 3.2 °C [*Flato et al.*, 2013], giving us confidence the projected temperature changes at our sites are not unreasonable relative to the full CMIP5 ensemble. To extract CCSM4 projection time series at the peatland site locations, we use the same process of bilinearly interpolating from the CCSM4 grid (0.9° x 1.25°) and applying CRU bias correction using the 1950-1990 CE climatology period. In our analysis and results below, HPM-Arctic is driven by TraCE-21ka output prior to 1990 CE and CCSM4 afterwards. The RCP8.5 simulations spans 2005 through 2100 CE.

Statistical analysis and data analysis

We used two basic statistical analyses in our evaluation of model results. We tested for differences between present day and future C stocks in the two scenarios (perched, flooded) across the sites using a t-test (R command: t.test). We used a paired t-test when comparing the differences between time periods (present-day, 2100 CE) to account for differences between the sites and scenarios. We tested several hypotheses for controls on total C loss in the future scenarios, including climatic conditions and changes (present-day observed mean annual temperatures and precipitation, projected air temperatures and precipitation from 2071-2100 CE, and the change between the two time periods), and some peat characteristics, including basal ages, peat C stocks in 2015 CE, and mean degree of peat decomposition across the peat profiles in 2015 CE. We used linear regressions between the changes in C stocks by 2100 CE and the predictor variables to test for significance of the predictors (R command: lm). All statistical analyses were conducted using R statistical software [R Core Development *Team*, 2008].

In order to compare modeled C losses with observations, we used the peat C stock in 2015 CE, and the results from old/new C tracker in 2100 CE. Net C loss (or gain) was calculated from the difference in total C stocks in 2015 and 2100 CE; mean annual rates were calculated by dividing the difference by Δt (85 years) and multiplying by 100 years century^{-1} for century rates.

Results and discussion

Model evaluation

At each site, the peat profiles simulated by HPM-Arctic were compared against peat core observations, including age-depth profiles. HPM-Arctic was able to reproduce the patterns of peat accumulation (i.e., peat age-depth profiles) at all sites using site-specific parameters related to hydrology and vegetation productivity (Figure 3, Table 2). The good agreement between the model and observations indicates that the model is capable of simulating realistic rates of peat accumulation and total peat height for sites across the northern permafrost region (Figure 3). The final peat height in present-day did not differ significantly between observed cores and the modeled profiles (t=-0.52, d.f.=9.6, *P*=0.61). The simulated organic matter density profile in the peat was in broad agreement with data from the peat cores across the sites, however HPM-Arctic profiles were always much smoother than observation (Figure S1). In particular, the model underestimated organic matter density near the peat surface (to about 20-40 cm depth) at several of the most northern sites (e.g., Ennadai, Baillie Bog, and TKP), and overestimated shallow peat bulk density at the southern site (JBL3). Mean modeled peat C stocks across the six sites did not differ significantly from the observational mean (mean modeled = 104 kg C m^{-2}; mean observed = 110 kg C m^{-2}; t=-0.41, d.f.=9.5, *P*= 0.69). The model had only partial success in simulating the dominant PFT composition of the peat profiles, and while the simulations generated peat that was a mix of all PFTs, the modeled profiles were predominantly moss (Table 3).

Table 3. Field observations and model results for present day (2015: means of 2006-2015 CE, control) and future scenarios (2100: means of 2091-2100 CE) for peat height, peat C stocks, water table level, maximum annual active layer thickness, and dominant vegetation types, both by productivity (e.g. mean decadal NPP of surface vegetation) and preserved in the peat core record.

Site	**Year / scenario**	**Scenario**	**Peat height** (m)	**Peat C** (kg C m^{-2})	**Water table level** (m below surf)	**Active layer thickness** (m)	**Dominant vegetation – NPP**	**Dominant vegetation – Peat**
JBL3	2008	Observed	2.44	105.0	-	NA		Woody/moss
	2015 – C	Control	2.30	120.2	0.07	NA	Sedge	Sedge
	2100 – P	Perched	2.22	117.3	0.20	NA	Shrub	Moss
Joey Lake	2001	Observed	3.00	154.0	(unknown)	(unknown)	-	-
	2015 – C	Control	2.72	138.3	0.20	2.22	Shrub	Moss
	2100 – P	Perched	2.63	135.6	0.35	> 2.63	Shrub	Moss
	2100 – F	Flooded	2.66	136.7	0.23	> 2.66	Shrub	Moss
Selwyn Lake	1993	Observed	1.97	84.9	(dry)	0.47	Shrub	Woody/moss
	2015 – C	Control	1.82	91.5	0.19	0.62	Shrub	Moss
	2100 – P	Perched	1.82	91.4	0.34	> 1.82	Shrub	Moss
	2100 – F	Flooded	1.82	91.6	0.24	> 1.82	Shrub	Moss
Ennadai Lake	2002	Observed	1.86	74.3	(dry)	0.41	Shrub	Woody/moss
	2015 – C	Control	1.81	83.5	0.27	0.73	Shrub	Moss
	2100 – P	Perched	1.78	82.4	0.40	0.87	Shrub	Moss
	2100 – F	Flooded	1.78	82.4	0.40	0.87	Shrub	Moss
Baillie Bog	1993/4	Observed	1.97	122.3	(0.40)	0.40	Shrub	Sedge/Shrub
	2015 – C	Control	1.88	96.8	0.06	0.85	Sedge	Moss
	2100 – P	Perched	1.85	95.6	0.21	0.66	Shrub	Moss
TKP	1993/4	Observed	1.93	107.5	(0.40)	0.40	Shrub	Sedge/Shrub
	2015 – C	Control	1.90	88.6	0.03	0.87	Sedge	Moss
	2100 – P	Perched	1.85	87.0	0.15	0.79	Sedge	Moss

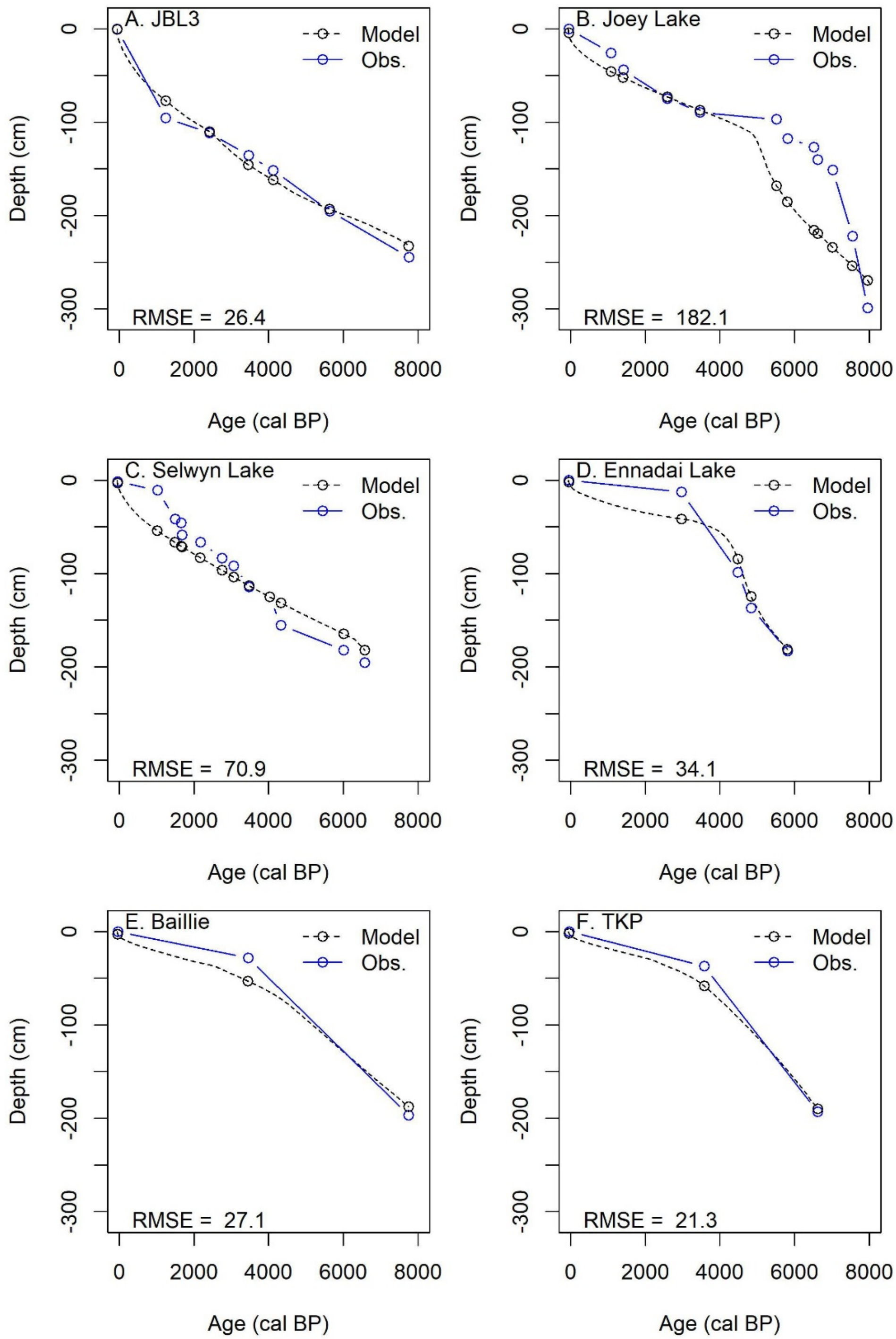

Figure 3. Model and observed age-depth profiles for cores in study, listed from south to north: A) JBL3, B) Joey Lake, C) Selwyn Lake, D) Ennadai Lake, E) Baillie Bog, F) TKP-Wet. RMSE represents root mean squared error of the difference between modeled and observed depths at the known radiocarbon age sampling points from the observations. Note that model age-depth profiles are continuous results, with labels added at depths of age observations in cores for comparison.

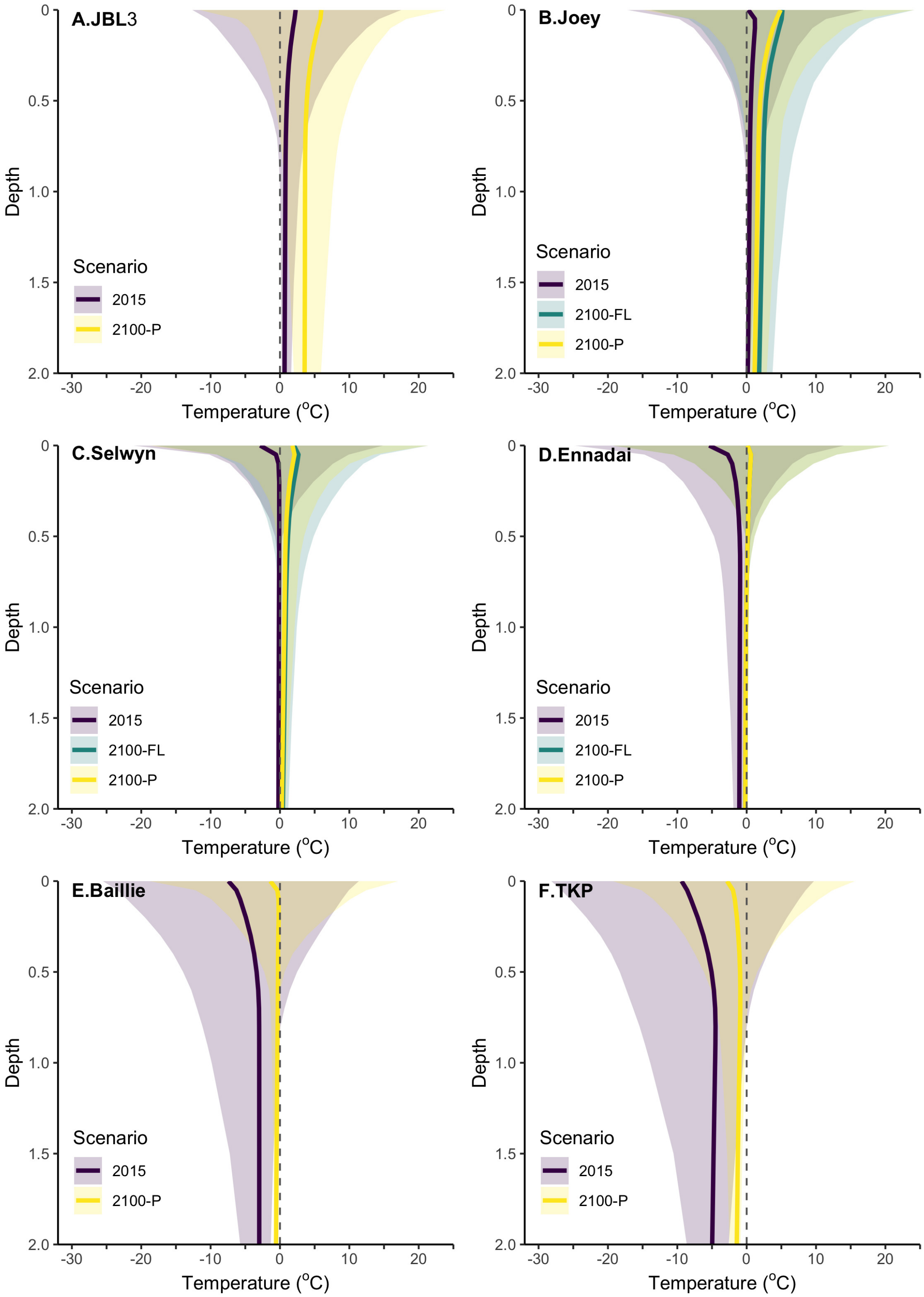

Figure 4. Distribution of modeled peat temperatures for 2006-2015 and 2091-2100 in A) JBL3, B) Joey Lake, C) Selwyn Lake, D) Ennadai Lake, E) Baillie Bog, and F) TKP. Heavy lines represent the mean annual peat temperatures, while the shaded areas represent the temperature range between the mean minimum annual and mean maximum annual peat temperature over the periods of interest. 'FL' and 'P' refer to flooded and perched water table scenarios (see text).

Model permafrost simulations and future projections

HPM-Arctic successfully simulated permafrost in the sites with permafrost and no permafrost in the permafrost-free site in the present day (Table 3). At JBL3, the site without permafrost, the surface peat experienced seasonal freezing but the deeper peats remained thawed throughout the year (Figure 4). In the permafrost sites, modeled active layer thickness ranged from 0.6 – 2.2 m (Table 3), which was generally deeper than observations (Table 3). Across the sites with permafrost, we simulated a mean of 47 ± 35 kg C m^{-2} (sd) or 44% of total C stocks in the active layer, while a mean of 52 ± 15 kg C m^{-2} or 56% was contained within the permafrost.

By 2100 CE, the predicted mean annual air temperatures under RCP8.5 reached above freezing at the southern three sites and were substantially warmer at the northern sites (Figure S2, Table S1). The projected warming increased the active layer thickness in several sites with permafrost after 2000 CE (Table 3), resulting in the complete thaw of permafrost within the peat profile at the two southern permafrost sites, Joey and Selwyn Lake (Figure 4), while active layer thickness increased at Ennadai after 2050 (Figure S3). Permafrost remained in the peat profile for the three northernmost sites (Figure 4), with projected active layer thickness becoming shallower at Baillie Bog and staying similar at TKP (Table 3; Figure S3). Projected precipitation changes by 2100 generally fell within the decadal ranges of modern precipitation amounts (Figure S4) but did increase by 2091-2100 relative to the present CRU data (Table S1). The projected warming increased modeled NPP across all sites after 2000 (Figure S5). In all sites, simulated NPP increased during the 21st century (Figure S5), ranging from 25% (Joey Lake) to nearly tripling (Selwyn Lake). At all sites, this was dominated by increases in woody (shrub) NPP, which increased by a mean of >200% across the sites.

HPM-Arctic simulated reduced net peat C stocks across all scenarios and sites by 2100 CE in response to 21st century warming (Figure 5). Across all sites, HPM predicted a loss of old peat accumulated before 2015 CE, ranging from -13.2 to -4.1 kg C m^{-2} between 2015 CE and 2100 CE. New peat was added from the additions of net primary productivity (Figure 5), which offset between 40% and 100% of C losses. Consequently, the net loss across the sites was predicted to be between -3.0 and +0.1 kg C m^{-2} by 2100 CE (Figure 5), with a mean loss of -1.6 kg C m^{-2}. This was a statistically significant decrease relative to C stocks in 2015 CE ($t=-4.5$, d.f.=9, $P= 0.002$; Table 3), but < 5% of the modeled peat C stocks at these sites. Median projected C loss from permafrost was -0.1 kg C m^{-2} by 2100 CE, and ranged from -1.7 kg C m^{-2} to -0.01 kg C m^{-2} (Figure 5). We hypothesized that the magnitude of net peat C loss throughout the profile in 2100 CE could be predicted by the climate drivers (temperature, precipitation), changes in the climate drivers, and the characteristics of the peat in 2015 CE. However, none of these factors were significant predictors of the magnitude of C stock change by 2100 CE ($P > 0.05$).

The model allowed us to examine the depth-distribution of C losses and gains in the peat profiles across the sites between 2015 CE and 2100 CE. Net C additions occurred in the surface 20 cm of peat in the three southernmost sites (JBL3, Joey Lake, Selwyn Lake, mean: +2.7± 1.4 kg C m-2), while losses of old C from the surface 20 cm were roughly equivalent to new C inputs in the northern sites (Ennadai, Baillie Bog, and TKP, mean: -0.2 ± 0.3 kg C m-2) resulting in a near-neutral C balance from the surface 20 cm of peat (Figure 6A,B). Across all sites, net C losses were greatest from 20-50 cm depths despite small additions of new C (Figure 6A,B); net losses ranged from -3.8 to -0.7 kg C m^{-2} an comprised 30-50% of losses of old C from the profile. Net C losses from 0.50-1.0 m depths were smaller (mean: -0.8 ± 0.6 kg C m^{-2}; range: -2.0 to -0.2 kg C m^{-2}) (Figure 6A,B). Losses of C from deep peats (> 1m depth) were generally very small (-0.2 to -0.0 kg C m^{-2}) with the exception of deep peat losses occurring in JBL3 and Selwyn Lake, which ranged from -0.8 to -0.7 kg C m^{-2} by 2100 CE (Figure 6A,B).

The two water table scenarios altered the hydrology towards drier conditions in the "perched" water table scenario and wetter conditions in the "flooded" water table scenario in the sites that experienced active layer deepening (Table 3). In the "perched" water table scenarios, the deepening of the active layer at Joey Lake, Selwyn Lake, and Ennadai Lake resulted in ~14 cm decrease in the water table (Table 3), which was essentially perched (constrained) atop the permafrost (Figure S3). While the net primary productivity of the herbaceous plant functional types and the total NPP were lower in the perched scenario than the flooded scenario (Figure S5), the thaw scenarios had little effect on the net C stocks (Figure 5). Compared with the "flooded" scenario, where the water table decreased by only 7 cm (Table 3), net peat C losses from the perched scenario were as much as -1.4 kg C m^{-2} larger than in the flooded scenarios by 2100 CE (Figure 5), but were not significantly different between the two scenarios ($t=-2.1$, d.f. = 3, $P = 0.13$). A comparison of net C change across peat depths for the two water table scenarios for Joey, Selwyn, and Ennadai Lake shows similar trends with depth across sites and only small differences in magnitudes of C losses and gains between the two scenarios (Figure 6A,B).

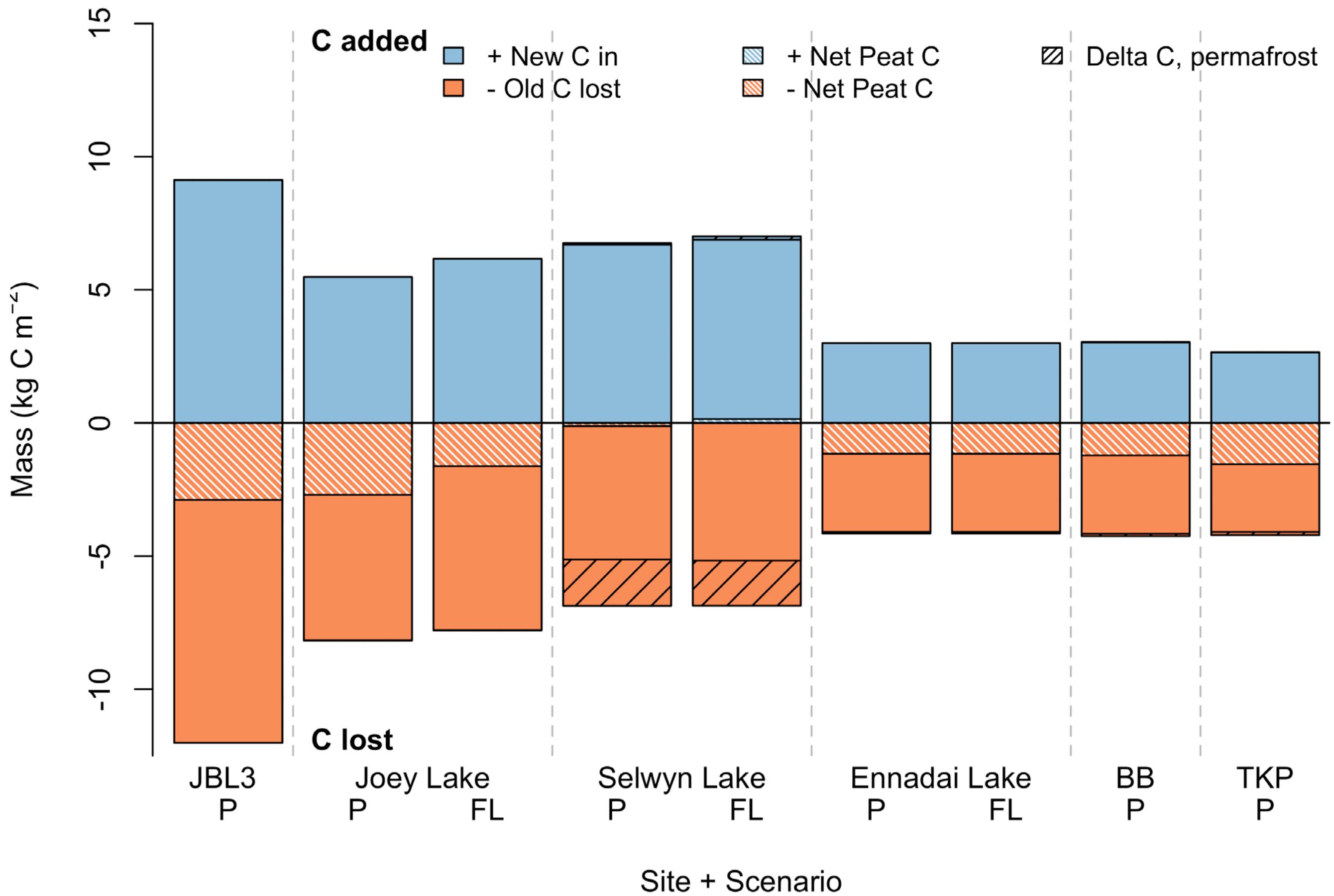

Figure 5. Change of modeled peat C stocks at the sites along the permafrost gradient between 2015 and 2100 under RCP8.5. "New" (blue) indicates the net C added to the peat through net primary productivity and lost from decomposition between 2015 and 2100, while "Old" (orange) indicates the total C fixed prior to 2015 that was lost between 2015 and 2100. Diagonal white shading indicates the magnitude of net change in peat C stocks due to old C losses and new C gains. Black diagonal lines indicate changes in permafrost C either from additions (black on blue) or losses (black on orange). Scenarios for all sites include perched water table ("P"), where the water table remains perched on top of the permafrost or mineral soil; flooded ("FL"), where the peat surface becomes flooded from localized runoff as permafrost thaws (see text; not triggered at all sites).

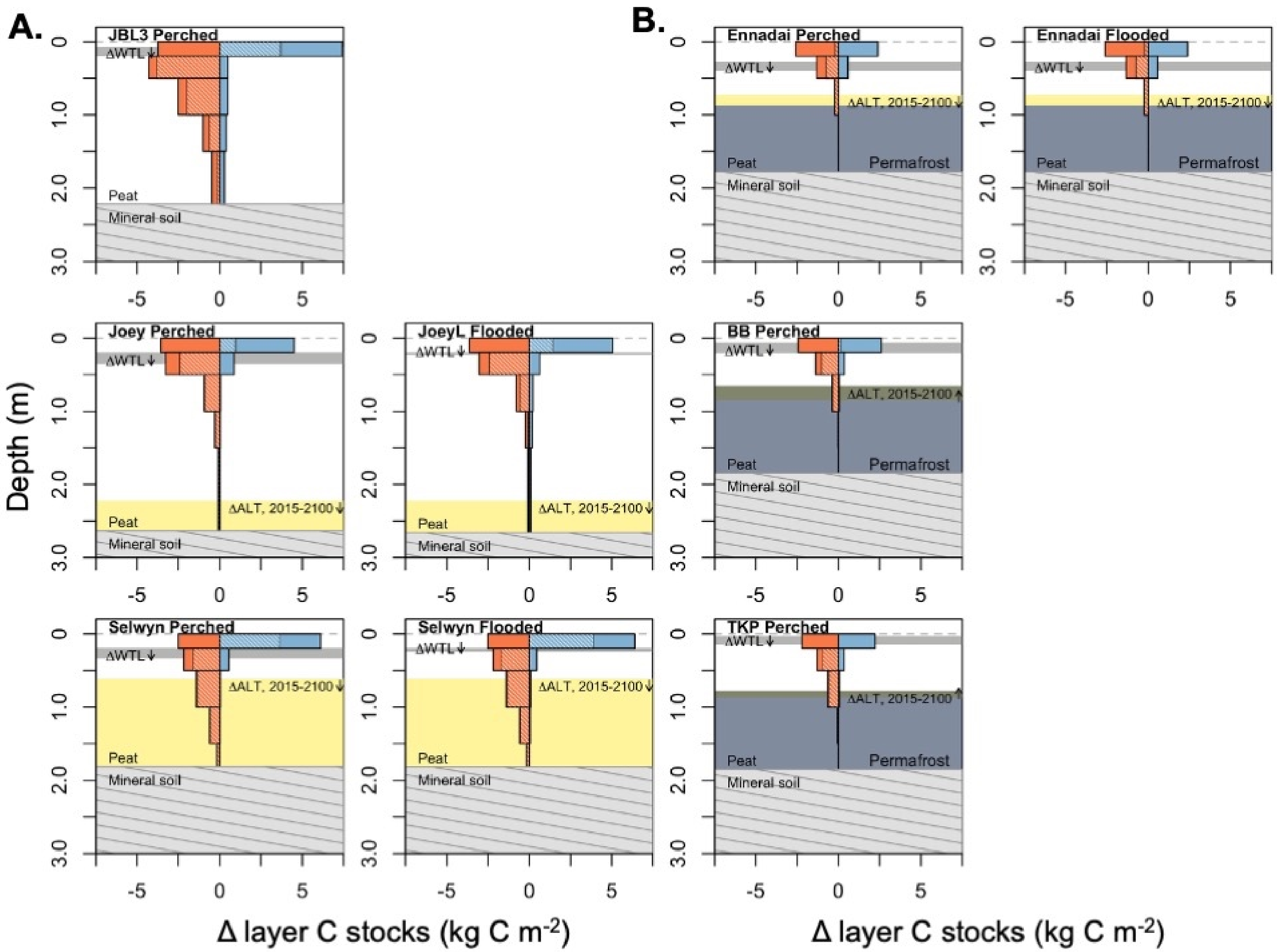

Figure 6. Change in peat C stocks between 2015 CE and 2100 CE by depth for the study sites. A) Southern sites including JBL3 (top), Joey Lake (middle), Selwyn (bottom) with perched water table scenarios in the left column and flooded (thermokarst) scenarios in the right column; B) northern sites including Ennadai (top), Baillie Bog (middle) and TKP (bottom). Losses of "old" C fixed before 2015 is shown in orange, net new added C after 2015 is in blue, the net of old C losses and net new C gains is shown by lighter orange and blue shaded areas. Changes in water table levels are indicated by horizontal gray bars and ΔWTL, changes in active layer thickness (e.g. permafrost thaw) are indicated by yellow zones and ΔALT, both for 2091-2100 relative to 2006-2015. Permafrost peat in 2100 CE is shown in blue-gray.

Discussion

Peatland and permafrost history as a driver of C loss post-thaw

A few empirical studies have quantified the potential for soil C loss following permafrost thaw in organic soils by combining site-level observational approaches with empirical modeling. A recent study based on repeated measurements projected (old) soil C losses ranging from -25 to -20 kg C m^{-2} $century^{-1}$ by 2100 for a tundra site in Alaska experiencing permafrost thaw [*Plaza et al.*, 2019]; HPM-Arctic simulated smaller losses of old C, ranging from -15.5 to -4.8 kg C m^{-2} $century^{-1}$. Using a chronosequence of thawed permafrost peatlands to account for the additions of new C to the peat profile as well as losses of old peat from deeper in the peat profile, *Jones et al.* [2017] estimated *net* loss rates of peat C from following thaw of -35 to -5 kg C m^{-2} $century^{-1}$ from boreal sites in Alaska. HPM-Arctic modeled range for *net* C loss rates (including net new C added and old C lost) across all permafrost sites in this study was -15.5 to + 0.2 kg C m^{-2} $century^{-1}$. These net C loss rates agree well with recent observations following thaw from a boreal permafrost peatland in Canada, which range from -10.6 kg C m^{-2} $century^{-1}$ to +2.7 kg C m^{-2} $century^{-1}$ [*Heffernan et al.*, 2020]. There is substantial disagreement among the different empirical results from these different sites, which may be due simply to site differences, but multi-site comparisons have shown underlying differences in substrate related to permafrost and peatland histories. The timing of permafrost aggradation relative to peat formation is hypothesized to be a major control on potential C loss from peatlands due to how decomposed the peat substrate is at the time when it is frozen [*Jones et al.*, 2017; *Treat et al.*, 2014].

HPM can be useful to investigate the hypothesis that the relative timing of peat deposition to permafrost aggradation controls C loss post-thaw. We quantified the length of time between peat deposition and the peat entering the permafrost in HPM, i.e., its residence time in the active layer and length of time the peat is subject to decomposition. In this permafrost transect study, only the two southern permafrost sites were projected to have meaningful permafrost thaw by 2100 CE, which would expose substantial previously frozen peat to decomposition. The model showed that permafrost thawed completely within the peat profile at these sites by 2100 CE (Figure 6A, Table 3) and the peat was subsequently vulnerable to decomposition. However, simulated net C lost from permafrost at Joey Lake was ~ 0 g C m^{-2} and 1.7 kg C m^{-2} at Selwyn by 2100 CE (Figure 5), while deeper peat losses from depths of 0.5 m to 1.5 m were 33-66% smaller at Joey Lake (-0.7 to -1.2 kg C m^{-2}) than at Selwyn Lake (-1.9 to -2.0 kg C m^{-2}; Figure 6A) despite warmer peat temperatures (Figure 4B,C). The modeled peat at Joey Lake in the 0.5 m to 1.5 m depths was slightly more decomposed than at Selwyn Lake (median: 89% mass lost vs. 87% mass lost), but a better explanation of the difference could be the length of the residence time that the peat was in the active layer and vulnerable to decomposition before being frozen into the permafrost. At Joey Lake, the peat between 0.5 m and 1.5 m was in the active layer for ~2250 years prior to being incorporated into permafrost, whereas at Selwyn Lake, the peat was incorporated into the permafrost after only 1200 years, limiting the length of time for decomposition in the past and increasing the vulnerability of permafrost. Thus, the amount of time peat resides in the active layer or prior to permafrost aggradation can influence the degree decomposition prior to incorporation into the permafrost and can subsequently dictate the amount of post-thaw carbon loss. Therefore, understanding the site history can be very important for projecting potential C loss with permafrost thaw.

Peat C vulnerability to warmer temperatures: Permafrost thawing acts as a buffer to warming

Site history is not the only important predictor of potential C loss in the future with climate warming and permafrost thaw. We initially hypothesized that projected peat C loss by 2100 CE would be greatest from sites that experienced a shift in mean annual air temperature from below freezing to above 0°C (e.g. Joey Lake and Selwyn Lake, Figure S2) because of the resulting permafrost thaw. While the magnitudes of net C losses were not significantly correlated with changes in environmental variables or peat characteristics, changes in peat temperature and moisture were the strongest at JBL3 (Figure 4, Table 3) despite having a smaller increase in air temperature than at more northern sites (+3.8 °C at JBL3 vs. +6.5 °C at Joey Lake; Table S1). At JBL3, warmer peat temperatures from 0.5 to 2 m depth (with a mean annual temperature of +3°C (range 0-6°C) for JBL3 by 2100 CE), which were substantially warmer than either Joey Lake (mean annual temperature +1.5°C, range 0-3°C by 2100 CE) or at Selwyn Lake (+0.5°C, Figure 4), were projected to lead to substantially more decomposition when persisting for decades [e.g. *Schädel et al.*, 2016]. This is reflected in the magnitude of both net C losses (Figure 5) and net C losses with depth at JBL3 (Figure 6A), which were much larger at this southern, permafrost-free site compared to the cooler sites. The presence of permafrost in peat, rather than enhance C loss with thaw, may instead have some potential to buffer peat C from decomposition in warming temperatures through the heat sink of phase change in thawing ice in permafrost peat and the underlying mineral soil and bedrock (e.g. Figure 4). This study showed smaller C losses from permafrost peats relative to peats without permafrost (Figure 5) despite larger air temperature increases due to phase change in frozen peat (Figure 4), which has also been shown recently more broadly across northern peatlands [*Chaudhary et al.*, 2020].

Key drivers of net peat carbon loss in observations and modeling: new peat additions vs. deeper peat losses

HPM-Arctic shows the importance of considering both C losses through enhanced decomposition and the role of new peat accumulation at sites. The comparison of the two water table scenarios, perched and flooded, at Joey, Selwyn, and Ennadai Lake demonstrate why net C losses are so difficult to predict based on simple drivers: net C additions plays an important role in offsetting decomposition losses, particularly in dynamic surface peats. Figure 6 shows the total old C losses throughout the peat profiles (orange), while new peat additions occur mainly in the surface peat. For Joey, Selwyn, and Ennadai Lake, the loss profiles (orange) look relatively similar between the perched and flooded water table scenarios (Figure 6A, 5B, right and left panels), while net C added (blue) is slightly larger in the flooded scenario across all sites (Figure 6, Figure 5). The net effect is a small reduction in the net C loss in the flooded scenario relative to the perched scenario (Figure 5). Studies based on measurements of net primary productivity and recent C accumulation rates in surface peat also showed a net increase in C storage in thawed permafrost peats relative to permafrost peat plateaus for western Canadian sites due to increased moisture and moss productivity [*Camill et al.*, 2001; *Turetsky et al.*, 2007], which was simulated by the model (Figure S5). However, little is known about how net primary productivity in peatlands changes in response to warming (and CO_2 fertilization) in either the short-term or long-term [*Frolking et al.*, 2011], introducing significant uncertainty into predictions of change in net C stocks with permafrost thaw across the pan-Arctic [*McGuire et al.*, 2018]. Recent experimental show that new C inputs do not compensate for enhanced decomposition losses due to peat warming [*Hanson et al.*, 2020].

These modeling results illustrate the difficulties in trying to quantify losses of permafrost C from peatlands using observations. HPM-Arctic shows that generally, net C additions occur in the surface peat to 20 cm (~ +15 g C m^{-2} y^{-1}), which could be observed using approaches to measure NPP and NEE in surface peats (Figure 6). However, accounting for C losses in the deeper peat (> 20 cm) changed the direction of net C fluxes (Figure 6), given that predicted net losses of peat between 20 cm and 1 m were substantial (~ -30 g C m^{-2} y^{-1}); roughly 15% (-5 g C m^{-2} y^{-1}) of this could be attributed to permafrost C loss (Figure 5). Approaches to quantify the response of peat C to changing environmental conditions need to account for changes beneath the surface peat, particularly in the near surface peat (20-50 cm).

Given the lag between the warmest annual temperatures and the warmest peat temperatures in deeper peat, deep peat and permafrost C losses could be highest in the fall and winter [*Estop-Aragonés et al.*, 2018b; *Webb et al.*, 2016] and may be difficult to capture with observations both due to timing and to the relatively small magnitude of net C losses compared with the large annual fluxes of GPP and ER. Additionally, we show that the contribution from permafrost and deep peat to net C losses are relatively small compared to the shallower peats (Figure 6), thus the signal could be easily swamped by ecosystem respiration in shallower peats.

Insights and opportunities in peatland modeling

HPM-Arctic combines a detailed process-based understanding of peat decomposition, hydrology, C dynamics, and now how these interact with soil temperature and permafrost dynamics to influence peat C accumulation and loss. For determining potential C losses in peatlands, a process-based simulation model provides an alternative framework to empirical models using the permafrost thaw chronosequences. A process model can explore consequences of different thaw scenarios, e.g., wetter or drier conditions (Figure 5, 6). The HPM-Arctic model can explicitly separate the fate of carbon fixed before or after a particular date, and so quantify loss of 'old' carbon and sequestration of 'new' carbon, providing additional insights into the carbon dynamics (e.g. Figure 6). Process-based models are of course limited by how well they represent the processes included, as well as any relevant processes that have not been included. For example, the higher surface OM density at the northern sites is not simulated by HPM-Arctic (Fig. S2), indicating that, in permafrost zones, there are likely processes in peat accumulation and/or physical processing that are not included in the model or other models. Another important dynamic that is not accounted for in this study is ice melt, a process not simulated in HPM-Arctic, which can cause a range of effects, from peat compaction due to porewater ice melt that can reduce active layer thickness [e.g. *Plaza et al.*, 2019] to abrupt, deep thaw in peatlands associated either with melting of ice in the peat profile or in the underlying mineral soil. This abrupt thaw processes occur in ice-rich permafrost deposits and can change deep peat temperatures and phase change from permafrost to liquid water in a matter of years, making 'old' carbon more vulnerable to loss more quickly, and has been a significant driver of C loss in other model simulations [e.g. *Nitzbon et al.*, 2020; *Schneider von Deimling et al.*, 2015; *Turetsky et al.*, 2020; *Walter Anthony et al.*, 2018].

This study shows that net C balance in peatlands in response to warming can result in a range of outcomes, from increased net C accumulation to net C losses. Across all sites, net C losses from active layer peat between 0.2 – 1.0 m depth were the predominant driver of total C loss between 2015-2100 CE, rather than losses from deeper peat (>1 m) or newly thawed permafrost. Across the sites, new peat accumulation offset a relatively large fraction of C losses, but the response of net primary productivity to temperature for many peatland species and plant functional types remains poorly understood and is an important area for future research. Factors such as site history, the presence/absence of permafrost in the present-day, and climatic factors are important to consider when trying to predict how C stocks will change with climate change in northern peatlands.

Acknowledgments

We thank S. Glidden for the study map and two anonymous reviewers for their feedback. This study was supported by the US National Science Foundation (#1802825, CCT & SF; NSF DEB 0092704, PC), ERC-StG #851181 FluxWIN (CCT), the Fulbright Finland and Saastamoinen Foundations (SF), USGS Land Change Science Program (JA, MCJ). We acknowledge field work and analysis done by J Holmquist (James Bay Lowlands (JBL3), Ontario) and SR Vardy (Baillie Bog, Northwest Territories, and Thelon-Kazan Peatlands, Nunavut). The model code, parameters, and climate driver data are available from: https://doi.org/10.5281/zenodo.4647666. TraCE-21ka was made possible by the DOE INCITE computing program, and supported by NCAR, the NSF P2C2 program, and the DOE Abrupt Change and EaSM programs.

References

Brown, J., O. Ferrians, J. A. Heginbottom, and E. S. Melnikov (2002), Circum-Arctic Map of Permafrost and Ground-Ice Conditions, Version 2., *NSIDC: National Snow and Ice Data Center*, *doi: https://nsidc.org/data/GGD318*, 7 May 2020, doi:doi: https://nsidc.org/data/GGD318.

Camill, P., A. Barry, E. Williams, C. Andreassi, J. Limmer, and D. Solick (2009), Climate-vegetation-fire interactions and their impact on long-term carbon dynamics in a boreal peatland landscape in northern Manitoba, Canada, *J. Geophys. Res.*, *114*, G04017, doi:10.1029/2009jg001071.

Camill, P., J. A. Lynch, J. S. Clark, J. B. Adams, and B. Jordan (2001), Changes in biomass, aboveground net primary production, and peat accumulation following permafrost thaw in the boreal peatlands of Manitoba, Canada, *Ecosystems*, *4*(5), 461-478, doi:DOI: 10.1007/s10021-001-0022-3.

Charman, D. J. (2002), *Peatlands and Environmental Change*, 301 pp., John Wiley & Sons, Chichester, UK.

Chaudhary, N., S. Westermann, S. Lamba, N. Shurpali, B. K. Sannel, G. Schurgers, P. A. Miller, and B. Smith (2020), Modelling past and future peatland carbon dynamics across the pan-Arctic, *Global Change Biology*, https://doi.org/10.1111/gcb.15099, doi:10.1111/gcb.15099.

Dorrepaal, E., S. Toet, R. van Logtestijn, E. Swart, M. J. van de Weg, T. V. Callaghan, and R. Aerts (2009), Carbon respiration from subsurface peat accelerated by climate warming in the subarctic, *Nature*, *460*, 616 - 619, doi:DOI: 10.1038/nature08216.

Estop-Aragonés, C., et al. (2018a), Limited release of previously-frozen C and increased new peat formation after thaw in permafrost peatlands, *Soil Biology and Biochemistry*, *118*, 115-129, doi:https://doi.org/10.1016/j.soilbio.2017.12.010.

Estop-Aragonés, C., C. I. Czimczik, L. Heffernan, C. Gibson, J. C. Walker, X. Xu, and D. Olefeldt (2018b), Respiration of aged soil carbon during fall in permafrost peatlands enhanced by active layer deepening following wildfire but limited following thermokarst, *Environmental Research Letters*, *13*(8), 085002, doi:10.1088/1748-9326/aad5f0.

Flato, G. M., et al. (2013), Evaluation of Climate Models, in *Climate Change 2013: The Physical Science Basis. Contribution of Working Group I to the Fifth Assess- ment Report of the Intergovernmental Panel on Climate Change*, edited by T. F. Stocker, D. Qin, G.-K. Plattner, M. Tignor, S. K. Allen, J. Boschung, A. Nauels, Y. Xia, V. Bex and P. M. Midgley, pp. 741 - 866, Cambridge University Press, Cambridge, UK.

Frolking, S., N. T. Roulet, E. Tuittila, J. L. Bubier, A. Quillet, J. Talbot, and P. J. H. Richard (2010), A new model of Holocene peatland net primary production, decomposition, water balance, and peat accumulation, *Earth Syst. Dynam.*, *1*(1), 115-167, doi:10.5194/esdd-1-115-2010.

Frolking, S., J. Talbot, M. C. Jones, C. C. Treat, J. B. Kauffman, E.-S. Tuittila, and N. Roulet (2011), Peatlands in the Earth's 21st century climate systems, *Environmental Reviews*, *19*, 371-396, doi:doi:10.1139/A11-014.

Gent, P. R., et al. (2011), The Community Climate System Model Version 4, *Journal of Climate*, *24*(19), 4973-4991, doi:10.1175/2011jcli4083.1.

Glaser, P. H., D. I. Siegel, J. P. Chanton, A. S. Reeve, D. O. Rosenberry, J. E. Corbett, S. Dasgupta, and Z. Levy (2016), Climatic drivers for multidecadal shifts in solute transport and methane production zones within a large peat basin, *Global Biogeochemical Cycles*, *30*(11), 1578-1598, doi:10.1002/2016gb005397.

Gorham, E. (1991), Northern Peatlands - Role in the Carbon-Cycle and Probable Responses to Climatic Warming, *Ecological Applications*, *1*(2), 182-195.

Gorham, E., C. Lehman, A. Dyke, J. Janssens, and L. Dyke (2007), Temporal and spatial aspects of peatland initiation following deglaciation in North America, *Quaternary Science Reviews*, *26*(3-4), 300-311, doi:10.1016/j.quascirev.2006.08.008.

Hanson, P. J., et al. (2020), Rapid Net Carbon Loss From a Whole-Ecosystem Warmed Peatland, *AGU Advances*, *1*(3), e2020AV000163, doi:https://doi.org/10.1029/2020AV000163.

Harris, I., P. D. Jones, T. J. Osborn, and D. H. Lister (2014), Updated high-resolution grids of monthly climatic observations – the CRU TS3.10 Dataset, *International Journal of Climatology*, *34*(3), 623-642, doi:10.1002/joc.3711.

Harris, S. A., H. M. French, J. A. Heginbottom, G. H. Johnston, B. Ladanyi, D. C. Sego, and R. O. van Everdingen (1988), Glossary of Permafrost and Related Ground-Ice Terms*Rep. Technical Memorandum No. 142*, 154 pp. pp, National Research Council of Canada, Ottawa.

Haynes, K. M., R. F. Connon, and W. L. Quinton (2018), Permafrost thaw induced drying of wetlands at Scotty Creek, NWT, Canada, *Environmental Research Letters*, *13*(11), doi:10.1088/1748-9326/aae46c.

Heffernan, L., C. Estop-Aragonés, K.-H. Knorr, J. Talbot, and D. Olefeldt (2020), Long-term impacts of permafrost thaw on carbon storage in peatlands: deep losses offset by surficial accumulation, *Journal of Geophysical Research: Biogeosciences*, *n/a*(n/a), e2019JG005501, doi:10.1029/2019JG005501.

Hicks Pries, C. E., R. S. P. van Logtestijn, E. A. G. Schuur, S. M. Natali, J. H. C. Cornelissen, R. Aerts, and E. Dorrepaal (2015), Decadal warming causes a consistent and persistent shift from heterotrophic to autotrophic respiration in contrasting permafrost ecosystems, *Global Change Biology*, *21*(12), 4508-4519, doi:10.1111/gcb.13032.

Holmquist, J. R., and G. M. MacDonald (2014), Peatland succession and long-term apparent carbon accumulation in central and northern Ontario, Canada, *The Holocene*, *24*(9), 1075-1089, doi:10.1177/0959683614538074.

Hugelius, G., et al. (2020), Large stocks of peatland carbon and nitrogen are vulnerable to permafrost thaw, *Proceedings of the National Academy of Sciences*, 201916387, doi:10.1073/pnas.1916387117.

Jones, M. C., J. Harden, J. O'Donnell, K. Manies, T. Jorgenson, C. Treat, and S. Ewing (2017), Rapid carbon loss and slow recovery following permafrost thaw in boreal peatlands, *Global Change Biology*, *23*(3), 1109-1127, doi:10.1111/gcb.13403.

Liu, Z., et al. (2009), Transient Simulation of Last Deglaciation with a New Mechanism for Bolling-Allerod Warming, *Science*, *325*(5938), 310-314, doi:10.1126/science.1171041.

Marchenko, S., V. Romanovsky, and G. Tipenko (2008), Numerical modeling of spatial permafrost dynamics in Alaska, paper presented at Ninth International Conference on Permafrost, Institute of Northern Engineering, University of Alaska Fairbanks, Fairbanks, AK.

McGuire, A. D., et al. (2018), Dependence of the evolution of carbon dynamics in the northern permafrost region on the trajectory of climate change, *Proceedings of the National Academy of Sciences*.

Nichols, J. E., and D. M. Peteet (2019), Rapid expansion of northern peatlands and doubled estimate of carbon storage, *Nature Geoscience*, doi:10.1038/s41561-019-0454-z.

Nitzbon, J., S. Westermann, M. Langer, L. C. P. Martin, J. Strauss, S. Laboor, and J. Boike (2020), Fast response of cold ice-rich permafrost in northeast Siberia to a warming climate, *Nature Communications*, *11*(1), 2201, doi:10.1038/s41467-020-15725-8.

O'Donnell, J. A., M. T. Jorgenson, J. W. Harden, A. D. McGuire, M. Kanevskiy, and K. P. Wickland (2012), The effects of permafrost thaw on soil hydrologic, thermal, and carbon dynamics in an Alaskan Peatland, *Ecosystems*, *15*, 213-229, doi:DOI: 10.1007/s10021-011-9504-0.

Olson, D. M., et al. (2001), Terrestrial Ecoregions of the World: A New Map of Life on Earth: A new global map of terrestrial ecoregions provides an innovative tool for conserving biodiversity, *BioScience*, *51*(11), 933-938, doi:10.1641/0006-3568(2001)051[0933:teotwa]2.0.co;2.

Osterkamp, T. E., M. T. Jorgenson, E. A. G. Schuur, Y. L. Shur, M. Z. Kanevskiy, J. G. Vogel, and V. E. Tumskoy (2009), Physical and ecological changes associated with warming permafrost and thermokarst in Interior Alaska, *Permafrost and Periglacial Processes*, *20*(3), 235-256, doi:DOI: 10.1002/ppp.656.

Osterkamp, T. E., L. Viereck, Y. Shur, M. T. Jorgenson, C. Racine, A. Doyle, and R. D. Boone (2000), Observations of thermokarst and its impact on boreal forests in Alaska, USA, *Arctic Antarctic and Alpine Research*, *32*(3), 303-315.

Plaza, C., et al. (2019), Direct observation of permafrost degradation and rapid soil carbon loss in tundra, *Nature Geoscience*, *12*(8), 627-631, doi:10.1038/s41561-019-0387-6.

Prater, J. L., J. P. Chanton, and G. J. Whiting (2007), Variation in methane production pathways associated with permafrost decomposition in collapse scar bogs of Alberta, Canada, *Global Biogeochemical Cycles*, *21*(4), GB4004.

Roessger, N., C. Wille, D. Holl, M. Goeckede, and L. Kutzbach (2019), Scaling and balancing carbon dioxide fluxes in a heterogeneous tundra ecosystem of the Lena River Delta, *Biogeosciences*, *16*(13), 2591-2615, doi:10.5194/bg-16-2591-2019.

Roulet, N. T., P. M. Lafleur, P. J. H. Richard, T. R. Moore, E. R. Humphreys, and J. Bubier (2007), Contemporary carbon balance and late Holocene carbon accumulation in a northern peatland, *Global Change Biology*, *13*(2), 397-411.

Rydin, H., and J. K. Jeglum (2006), *Biology of Peatlands*, Oxford University Press, Oxford, UNITED KINGDOM.

Sannel, A. B. K., and P. Kuhry (2008), Long-term stability of permafrost in subarctic peat plateus, west-central Canada, *The Holocene*, *18*(4), 589-601.

Sannel, A. B. K., and P. Kuhry (2009), Holocene peat growth and decay dynamics in sub-arctic peat plateaus, west-central Canada, *Boreas*, *38*(1), 13-24, doi:10.1111/j.1502-3885.2008.00048.x.

Schädel, C., et al. (2016), Potential carbon emissions dominated by carbon dioxide from thawed permafrost soils, *Nature Climate Change*, *6*(10), 950-953, doi:10.1038/nclimate3054.

Schneider von Deimling, T., G. Grosse, J. Strauss, L. Schirrmeister, A. Morgenstern, S. Schaphoff, M. Meinshausen, and J. Boike (2015), Observation-based modelling of permafrost carbon fluxes with accounting for deep carbon deposits and thermokarst activity, *Biogeosciences*, *12*(11), 3469-3488.

Schuur, E. A. G., et al. (2015), Climate change and the permafrost carbon feedback, *Nature*, *520*(7546), 171-179, doi:10.1038/nature14338.

Seppälä, M. (2011), Synthesis of studies of palsa formation underlining the importance of local environmental and physical characteristics, *Quaternary Research*, *75*(2), 366-370, doi:http://dx.doi.org/10.1016/j.yqres.2010.09.007.

Tarnocai, C. (2006), The effect of climate change on carbon in Canadian peatlands, *Global and Planetary Change*, *53*(4), 222-232.

Taylor, K. E., R. J. Stouffer, and G. A. Meehl (2012), An Overview of CMIP5 and the Experiment Design, *Bulletin of the American Meteorological Society*, *93*(4), 485-498, doi:10.1175/bams-d-11-00094.1.

Team, R. D. C. (2008), R: A language and environment for statistical computing, edited, R Foundation for Statistical Computing, Vienna, Austria.

Treat, C. C., and M. C. Jones (2018), Near-surface permafrost aggradation in Northern Hemisphere peatlands shows regional and global trends during the past 6000 years, *The Holocene*, 0959683617752858, doi:10.1177/0959683617752858.

Treat, C. C., et al. (2016), Effects of permafrost aggradation on peat properties as determined from a pan-Arctic synthesis of plant macrofossils, *Journal of Geophysical Research: Biogeosciences*, *121*(1), 78-94, doi:10.1002/2015JG003061.

Treat, C. C., et al. (2018), Tundra landscape heterogeneity, not interannual variability, controls the decadal regional carbon balance in the Western Russian Arctic, *Global Change Biology*, *24*(11), 5188-5204, doi:10.1111/gcb.14421.

Treat, C. C., D. Wisser, S. Marchenko, and S. Frolking (2013), Modelling the effects of climate change and disturbance on permafrost stability in northern organic soils, *Mires and Peat*, *12*, Article 02: 01-17.

Treat, C. C., W. M. Wollheim, R. K. Varner, A. S. Grandy, J. Talbot, and S. Frolking (2014), Temperature and peat type control CO2 and CH4 production in Alaskan permafrost peats, *Global Change Biology*, *20*(8), 2674–2686, doi:10.1111/gcb.12572.

Turetsky, M. R., et al. (2020), Carbon release through abrupt permafrost thaw, *Nature Geoscience*, *13*(2), 138-143, doi:10.1038/s41561-019-0526-0.

Turetsky, M. R., R. K. Wieder, D. H. Vitt, R. J. Evans, and K. D. Scott (2007), The disappearance of relict permafrost in boreal north America: Effects on peatland carbon storage and fluxes, *Global Change Biology*, *13*(9), 1922-1934.

Vardy, S. R., B. G. Warner, and T. Asada (2005), Holocene environmental change in two polygonal peatlands, south-central Nunavut, Canada, *Boreas*, *34*(3), 324-334.

Vardy, S. R., B. G. Warner, J. Turunen, and R. Aravena (2000), Carbon accumulation in permafrost peatlands in the Northwest Territories and Nunavut, Canada, *Holocene*, *10*(2), 273-280.

Walter Anthony, K., T. S. von Deimling, I. Nitze, S. Frolking, A. Emond, R. Daanen, P. Anthony, P. Lindgren, B. Jones, and G. Grosse (2018), 21st-century modeled permafrost carbon emissions accelerated by abrupt thaw beneath lakes, *Nature communications*, *9*(1), 1-11.

Webb, E. E., E. A. G. Schuur, S. M. Natali, K. L. Oken, R. Bracho, J. P. Krapek, D. Risk, and N. R. Nickerson (2016), Increased wintertime CO2 loss as a result of sustained tundra warming, *Journal of Geophysical Research: Biogeosciences*, *121*(2), 249-265, doi:10.1002/2014JG002795.

Wisser, D., S. Marchenko, J. Talbot, C. Treat, and S. Frolking (2011), Soil temperature response to 21st century global warming: the role of and some implications for peat carbon in thawing permafrost soils in North America, *Earth Syst. Dynam.*, *2*(1), 121-138, doi:DOI: 10.5194/esd-2-121-2011.

Zoltai, S. C. (1993), Cyclic Development of Permafrost in the Peatlands of Northwestern Alberta, Canada, *Arctic and Alpine Research*, *25*(3), 240-246.

Zoltai, S. C., and D. H. Vitt (1990), Holocene Climatic-Change and the Distribution of Peatlands in Western Interior Canada, *Quaternary Research*, *33*(2), 231-240.